

Technical University of Denmark



Core Flooding Experiments and Reactive Transport Modeling of Seasonal Heat Storage in the Hot Deep Gassum Sandstone Formation

Holmslykke, Hanne D.; Kjøller, Claus; Fabricius, Ida Lykke

Published in:
Acs Earth and Space Chemistry

Link to article, DOI:
[10.1021/acsearthspacechem.7600031](https://doi.org/10.1021/acsearthspacechem.7600031)

Publication date:
2017

Document Version
Peer reviewed version

[Link back to DTU Orbit](#)

Citation (APA):
Holmslykke, H. D., Kjøller, C., & Fabricius, I. L. (2017). Core Flooding Experiments and Reactive Transport Modeling of Seasonal Heat Storage in the Hot Deep Gassum Sandstone Formation. *Acs Earth and Space Chemistry*, 1(5), 251-260. DOI: 10.1021/acsearthspacechem.7600031

DTU Library
Technical Information Center of Denmark

General rights

Copyright and moral rights for the publications made accessible in the public portal are retained by the authors and/or other copyright owners and it is a condition of accessing publications that users recognise and abide by the legal requirements associated with these rights.

- Users may download and print one copy of any publication from the public portal for the purpose of private study or research.
- You may not further distribute the material or use it for any profit-making activity or commercial gain
- You may freely distribute the URL identifying the publication in the public portal

If you believe that this document breaches copyright please contact us providing details, and we will remove access to the work immediately and investigate your claim.

1
2
3
4
5
6
7 1 Core flooding experiments and reactive transport
8
9
10
11 2 modelling of seasonal heat storage in the hot deep
12
13
14
15 3 Gassum Sandstone Formation
16
17
18
19
20

21 4 *Hanne D. Holmslykke^{*a}, Claus Kjøller^b and Ida L. Fabricius^c*
22
23

24 5 ^aDepartment of Reservoir Geology, Geological Survey of Denmark and Greenland, Øster
25
26 6 Voldgade 10 DK-1350 Copenhagen K, Denmark
27
28
29

30 7 ^bDepartment of Geochemistry, Geological Survey of Denmark and Greenland, Øster Voldgade 10
31
32 8 DK-1350 Copenhagen K, Denmark
33
34

35 9 ^cDepartment of Civil Engineering, Technical University of Denmark, Brovej 118, DK-2800 Kgs
36
37 10 Lyngby, Denmark
38
39
40

41 11 KEYWORDS High temperature aquifer thermal energy storage, Deep aquifer thermal energy
42
43 12 storage, Reactive transport modelling, Flooding experiments, Gassum Formation
44
45
46
47
48
49
50
51
52
53
54
55
56
57
58
59
60

18 **ABSTRACT**

19 Seasonal storage of excess heat in hot deep aquifers is considered to optimise the usage of
20 commonly available energy sources. The chemical effects of heating the Gassum Sandstone
21 Formation to up to 150°C is investigated by combining laboratory core flooding experiments with
22 petrographic analysis and geochemical modelling. Synthetic formation water is injected into two
23 sets of Gassum Formation samples at 25°C, 50°C (reservoir temperature), 100°C and 150°C with
24 a velocity of 0.05 PV/hr and 0.1 PV/hr, respectively. Results show a significant increase in the
25 aqueous concentration of silicium and iron with increasing temperature due to dissolution of silica
26 and siderite. Increasing the reservoir temperature from 50°C to 100°C enhanced the naturally
27 occurring weathering of Na-rich feldspar to kaolinite. Dissolution of quartz increased sharply
28 above 100°C and was the dominating process at 150°C, resulting in a significant increase in the
29 aqueous silicium concentration. At temperatures $\leq 100^\circ\text{C}$, the silicium concentration was
30 controlled by a quasi-stationary state between feldspar dissolution and kaolinite precipitation while
31 the concentration was kinetically controlled by quartz dissolution at 150°C. Furthermore, a strong
32 coupling between dissolution, precipitation and flow velocity was observed.

33 The results of this study show that the effects of heat storage of up to 150°C in the Gassum
34 Formation in the Stenlille area is expected to have only minor effects on the properties of the
35 reservoir and that storage of excess heat in the Gassum Formation in the Stenlille area may be
36 possible provided operational precautions are taken.

37

38

39

1. INTRODUCTION

A temporal mismatch typically exists between the supply and the demand for heat. For example, during the summer excess heat is produced from waste incineration, while the demand for energy peaks during the winter. Seasonal storage of surplus heat in the subsurface may overcome this incongruity between supply and demand for heat. During summer, formation water is extracted from the aquifer and heated using the available surplus energy prior to reinjection into the reservoir. During winter, the stored hot water is extracted and used for district heating.

In Denmark, geothermal energy for district heating is already being extracted from deep sandstone aquifers with temperatures up to 75°C¹. Consequently, the possibility of seasonally storing excess heat in these geothermal aquifers is considered. Due to a relatively high *in situ* temperature combined with a low aquifer flow rate, the heat loss may be minimised in these aquifers. Furthermore, the heat storage may increase the heat potential in the aquifers and possibly prolong the life time of the geothermal aquifer^{2, 3}.

Heat storage in geothermal aquifers will inevitably increase the temperature of the aquifer.

Temperature is known to exert an important control on both the extent and rate of reactions of minerals in the aquifer. Generally, elevated temperatures increase reaction rates, while mineral solubility can either increase or decrease, depending on the thermodynamic properties of the mineral⁴⁻⁹. For example, increasing the temperature leads to higher solubility of silicates, but lower solubility of carbonates. The exponential dependence of reaction rates on temperature implies that the effects of the temperature becomes more pronounced at higher temperature differences^{4, 10}. Dissolution/precipitation processes in the aquifer may affect the permeability of the aquifer by changing the pore space geometry and pore connectivity¹¹⁻¹³. Furthermore, dissolution of the cementing material in the aquifer may reduce the mechanical strength of the

1
2
3
4 63 aquifer. A major concern is therefore that heat storage may permanently damage the aquifer
5
6 64 making extraction of further geothermal energy unfeasible.
7

8
9 65 Aquifer thermal energy storage systems in shallow aquifers injecting water with a temperature of
10
11 66 up to approximately 20°C and small temperature differences ($\Delta T < 15^\circ\text{C}$) are operating
12
13 67 successfully in many countries^{3, 14, 15}. Experiences with higher operational temperatures (up to
14
15 68 150°C) are less frequently reported^{6, 7, 16, 17}. Laboratory¹⁸⁻²² and field^{7, 16} tests show that the
16
17 69 release of silicium increases sharply at elevated temperatures due to the dissolution of quartz and
18
19 70 feldspars, while precipitation of several secondary minerals, including kaolinite, boehmite,
20
21 71 gibbsite, montmorillonite has been observed. Field tests of heat storage in confined shallow
22
23 72 sandstone aquifers at temperatures up to 150°C^{7, 16} revealed, however, calcium carbonate
24
25 73 precipitation as the critical water chemistry problem. Softening of the water before heating was
26
27 74 necessary to prevent scaling in the heat exchanger and storage well for successful operation of
28
29 75 the heat storage. A deep aquifer thermal energy storage system injecting surplus heat at a depth
30
31 76 of approximately 1200 m at a temperature of 90°C is operating successfully in Neubrandenburg,
32
33 77 Germany¹⁷.
34
35
36
37
38
39

40 78 Though the chemical reactions that potentially occur when heated formation water is injected
41
42 79 into the aquifer to a large extent is known, the rate, extent and coupling of these reactions are
43
44 80 highly site specific. In this study the potential geochemical reactions due to heat storage of up to
45
46 81 150°C in the deep subsurface of Denmark is investigated. Core flooding experiments combined
47
48 82 with petrographic analysis and geochemical modelling is conducted to identify the primary
49
50 83 chemical reactions that potentially occur when heated formation water is injected into the
51
52 84 aquifer. As a case study the Upper Triassic – Lower Jurassic Gassum Formation in the Stenlille
53
54 85 area is used because the Gassum Formation is the most widespread geothermal aquifer in
55
56
57
58
59
60

1
2
3 86 Denmark. As calcite cement is extremely rare in the Gassum Formation in the Stenlille area, heat
4
5
6 87 storage in this area may be viable since the operational problems caused by precipitation of
7
8 88 calcite upon cooling of the formation water may be avoided or at least minimised.
9

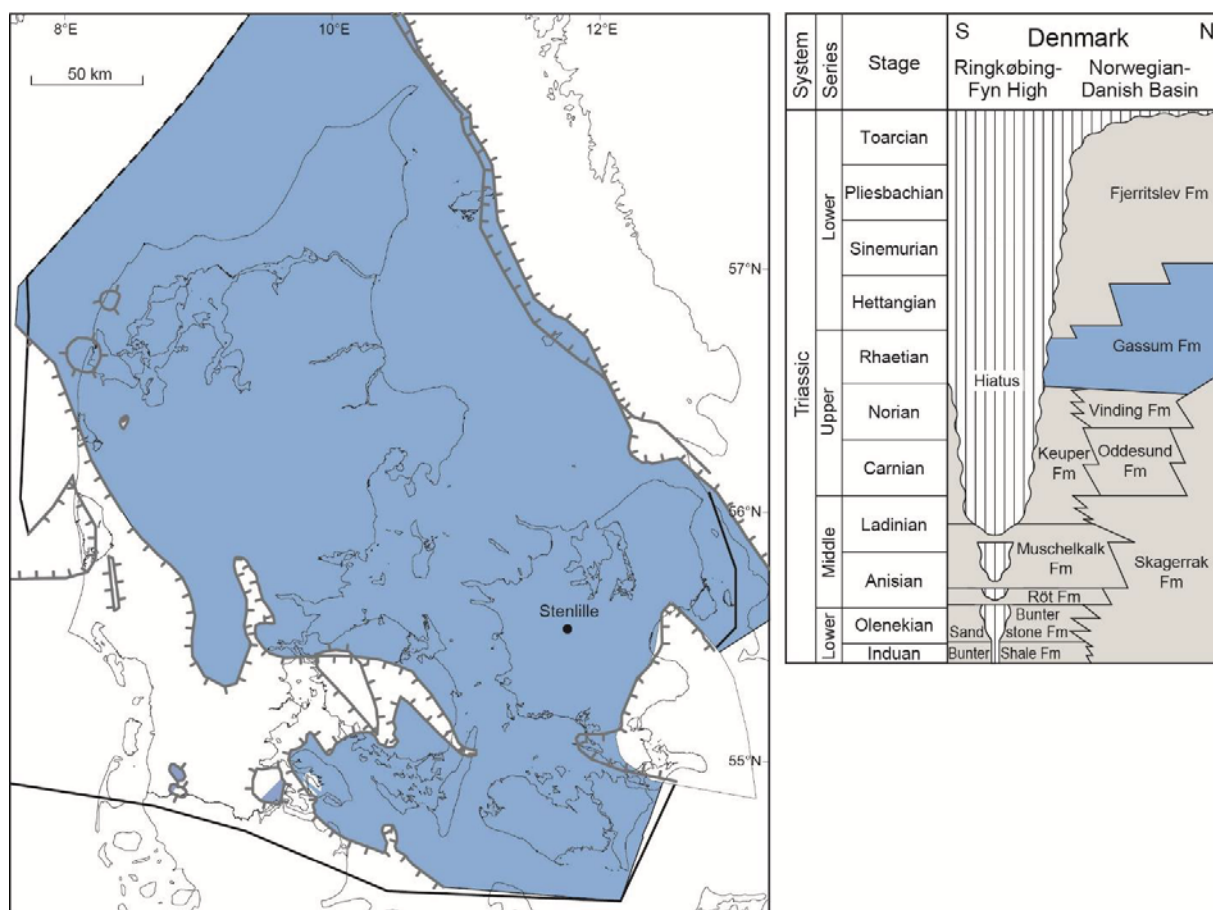
10 11 89 **2. MATERIALS AND METHODS**

12
13 90 **2.1. Geological background.** The Gassum Formation is present in most of the Danish area
14
15
16 91 (Figure 1) at a burial depth of 850 to 3350 m and is one of the most abundant Danish geothermal
17
18 92 reservoirs. The deposition initiated during the Upper Triassic 209 mio years ago and continued
19
20 93 during a series of relative sea level falls²³. Thus, the Gassum Formation consists of several
21
22 94 regressive shoreface and fluvial sandstones of wide lateral extent interbedded with mudstones
23
24 95 deposited in either marine, lagoonal and lacustrine environments²³. The thickness of the Gassum
25
26 96 Formation varies from 50 – 150 m in the Danish area, though thicknesses up to 300 m occur
27
28 97 locally due to salt structures and major faults^{23, 24}. The Gassum Formation forms an anticlinal
29
30 98 structure with a vertical closure of 35 m covering an area of 14 km² in the Stenlille area²⁵. The
31
32 99 individual reservoir intervals of well to moderately sorted, fine to medium-grained sandstone are
33
34
35
36
37 100 typically 10 m thick in the Stenlille area, though may be up to 60 m thick beneath the structural
38
39 101 closure.
40

41
42 102 The Gassum Formation is directly overlain by thick (up to 1000 m) marine mudstones of the
43
44 103 Lower Jurassic Fjerritslev Formation with large lateral continuity in the Danish part of the
45
46 104 Norwegian–Danish Basin, a thinner (few hundred metres) Middle Jurassic – Lower Cretaceous
47
48 105 succession and a thick (up to 2000 m) Upper Cretaceous chalk/limestone succession^{23, 26}. The
49
50 106 Gassum Formation overlies the restricted marine mudstones of the Upper Triassic Vinding
51
52
53 107 Formation and is covered by the marine mudstones of the Lower Jurassic Fjerritslev Formation.
54
55
56
57
58
59
60

1
2
3
4 108 The sandstones of the Gassum Formation are mainly subarkoses and arkoses²⁷ according to the
5
6 109 classification by McBride (1963)²⁸. The quartz content is highest in sandstones from the Stenlille
7
8 110 area, whereas cored intervals from Jutlandic wells show higher contents of feldspar and rock
9
10 111 fragments. The Gassum Formation at the Stenlille area has a very mature mineralogical
11
12 112 composition and calcite cement is extremely rare. Organic matter is typically not observed in
13
14 113 samples from the Stenlille area, although one sample showed an organic matter content of 6%.
15
16
17
18
19
20
21
22
23
24
25
26
27
28
29
30
31
32
33
34
35
36
37
38
39
40
41
42
43
44
45
46
47
48
49

114



115

116 **Figure 1.** Map of Denmark showing the extent of the Gassum Formation in blue colour (to the
117 left) and the stratigraphic scheme (to the right). Modified from²⁹

118

1
2
3
4 119 **2.2. Sample description and fluid.** In order to represent one of the most abundant Danish
5
6 120 geothermal reservoirs, two cylindrical specimens ($S_{0.05}$ and $S_{0.1}$) were prepared from a cored
7
8 121 interval of the Upper Triassic – Lower Jurassic Gassum Formation in the Stenlille-2 well (Figure
9
10 122 1). The tested samples had the approximate length and diameter of 74.5 mm and 38.0 mm,
11
12 123 respectively, and were selected from the same depth in the core (1539.50 m) to ensure close
13
14 124 similarity. The temperature of the reservoir is approximately 50°C, and the porosity (Φ), gas
15
16 125 permeability (K_g) and Klinkenberg permeability (K_L) of the two samples prior to testing were
17
18 126 $\Phi_{S_{0.05}} = 29.11\%$, $K_{g,S_{0.05}} = 195$ mD, $K_{L,S_{0.05}} = 183$ mD and $\Phi_{S_{0.1}} = 28.85\%$, $K_{g,S_{0.1}} = 181$ mD,
19
20 127 and $K_{L,S_{0.1}} = 177$ mD, respectively.
21
22
23
24 128 QEMSCAN[®] analysis of two samples from the same depth (1539.0 m) as the tested samples show
25
26 129 that the Gassum Formation primarily consists of quartz (72 % of solid) and secondarily of feldspar
27
28 130 (8% K-feldspar and 2.5% Na-feldspar) with minor contributions from kaolinite, mica, siderite and
29
30 131 heavy minerals. The QEMSCAN[®] analysis is thus in line with previous observations of the
31
32 132 mineralogy of the Gassum Formation³⁰.
33
34
35
36
37
38
39
40
41
42
43
44
45
46
47
48
49
50
51
52
53
54
55
56
57
58
59
60

134 **Table 1. Chemical composition of the synthetic Gassum brine used in the experiments in**
 135 **this study. The brine has been modified from³¹.**

	Concentration (mg/L)
Na	59,000
K	1,100
Mg	1,600
Ca	11,500
Sr	660
Cl	116,329
HCO ₃ ⁻	80
SO ₄ ²⁻	30

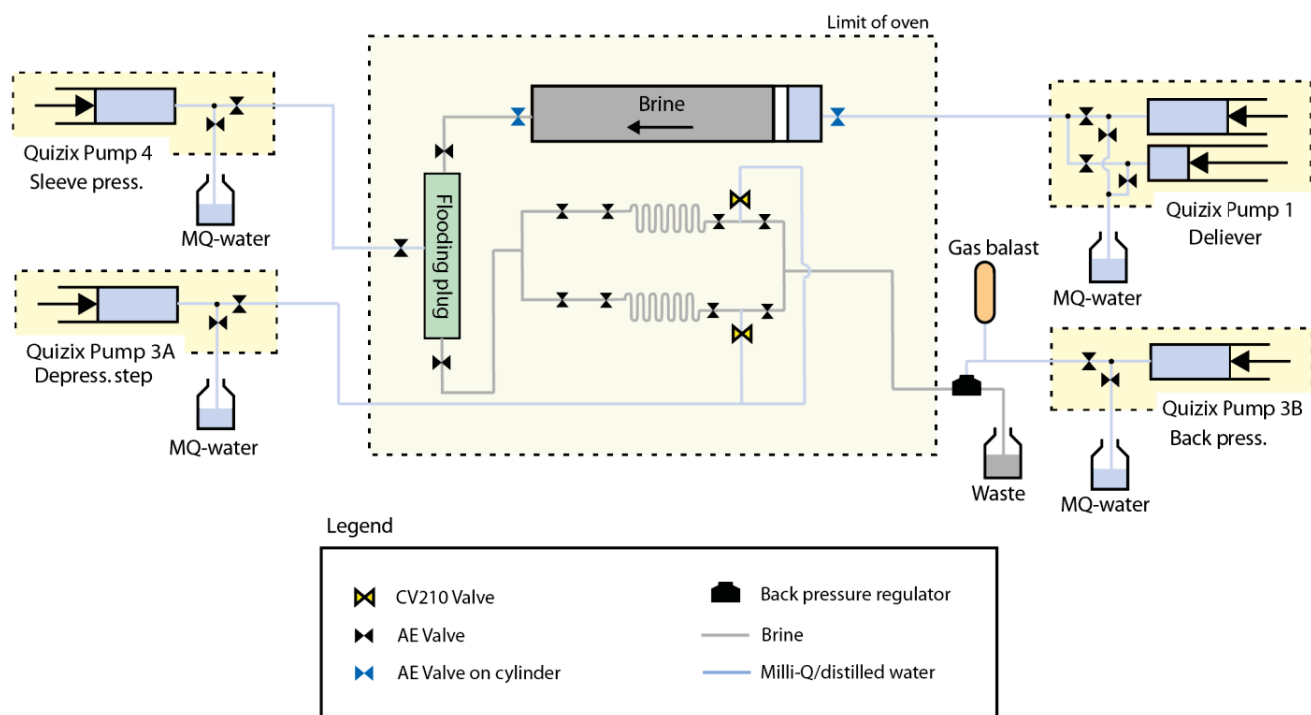
136
 137 The chemical composition of the Gassum flooding brine is modified from Laier (2008)³¹ and is
 138 shown in Table 1. The brine salinity is 17.02% with sodium and chloride being the dominating
 139 ions while calcium, magnesium and potassium also are present in significant amounts. The silicium
 140 and aluminium concentrations were not measured by Laier (2008)³¹. Initial chemical speciation
 141 calculations with PHREEQC³² using the Pitzer and the Thermodem³³ databases show in both cases
 142 that the Gassum brine is subsaturated with respect to sulphates such as anhydrite and celestine and
 143 to carbonates such as calcite and dolomite at all temperatures applied in the experiments.

144 **2.3. Experimental procedure.** In all, two core flooding experiments were performed such that
 145 one experiment was performed with each of the two specimens from the Gassum Formation.
 146 Synthetic Gassum brine was used as the flooding fluid, and flow velocities of 0.05 PV/hr (0.014
 147 cm/hr) and 0.1 PV/hr (0.029 cm/hr) were applied for specimens S_{0.05} and S_{0.1}, respectively. Prior

1
2
3
4 148 to testing, the specimens were cleaned in methanol to remove any salts precipitated from pore
5
6 149 water. He-porosity, N₂-gas permeability and Klinkenberg permeability were measured prior to and
7
8 150 after testing³⁴. Mineralogical changes in the specimens were identified by thin section analyses
9
10 151 using optical microscope and backscatter electron microscopy prior to and after the flooding
11
12 152 experiments to identify major chemical reactions responsible for the observed changes in aqueous
13
14 153 chemistry. The mineralogical observations provide information for the geochemical modelling.
15
16 154 Prior to testing, the specimens were vacuum (at -1 mbar) and pressure (at 110 bar for three days)
17
18 155 saturated in degassed formation water and the saturation state of the specimens was verified using
19
20 156 the Archimedes test.
21
22
23
24

25 157 The experimental set up is illustrated in Figure 2. The brine saturated specimen was placed in a
26
27 158 Viton sleeve inside a hydrostatic core holder and a confining pressure of 275 bar corresponding to
28
29 159 the *in situ* pressure was applied. *In situ* pore pressure was assured by impressing a back pressure
30
31 160 of 170 bar. A constant flow rate of either 0.05 PV/hr or 0.1 PV/hr was assured by high precision
32
33 161 Quizix[®] pumps in two parallel experiments in the same oven. For both flow rates, tests were
34
35 162 performed at 23°C, 50°C (reservoir temperature), 100°C and 150°C allowing flow for minimum
36
37 163 one week at each temperature. Downstream the core holder, each of the flow lines was equipped
38
39 164 with two sampling loops to collect effluent brine for chemical analysis. During sampling, flow was
40
41 165 allowed to pass through one of the two loops. When sampling, the flow was shifted to the empty
42
43 166 loop, and the loop with brine was dismantled from the oven and cooled fast to ambient temperature
44
45 167 (23±1°C) before transferring the content of the loop to a syringe. Sampling from both flowlines
46
47 168 (0.05 PV/hr and 0.1 PV/hr) was performed concomitantly in order to minimize temperature
48
49 169 oscillation in the oven. After sampling, the loop was filled with distilled water, placed in the oven
50
51 170 again and re-pressurised to 170 bar by injection of distilled water.
52
53
54
55
56
57
58
59
60

171



172

173 **Figure 2.** Experimental set up

174 The alkalinity and pH were measured immediately after sampling on unfiltered samples. The
 175 alkalinity was determined by Gran-titration³⁵. The rest of the sample was passed through 0.22 μm
 176 cellulose-acetate syringe filter into three separate polyethylene vials. Samples for cation and
 177 silicium analysis received 1 vol% of 7M HNO_3 and 10 vol% of 5M NaOH , respectively, and was
 178 kept refrigerated until ICP-MS analysis (PerkinElmer Elan6100DRC Quadrupol) with a standard
 179 deviation of 3-15% depending on the element measured. Samples for anion analysis (chloride and
 180 sulphate) were frozen until ion-chromatography analysis (LC50-CD50, Dionex, CA, USA) with a
 181 quantification limit of 0.05 mg/L.

182 **2.2 Reactive transport modelling.** The injection of heated formation water into the Gassum

183 Formation was modelled using the 1D reactive transport code PHREEQC version 3.0³².

184 Combined with the petrographic analysis, the hydrogeochemical modelling helps identify which

1
2
3 185 minerals may possibly dissolve and/or precipitate when heated Gassum brine is injected into the
4
5 186 Gassum Formation. A 1D transport model column, comprising 10 cells with a length of 0.0745
6
7 187 m each, was constructed and flushed with synthetic Gassum brine (Table 1) at 23°C, 50°C 100°C
8
9 188 and 150°C and at 170 bar pressure. Dispersion was not taken into account in the model. The
10
11 189 thermodynamic data from the Thermoddem database were used since this database is optimised
12
13 190 to high temperatures and includes a large range of silica minerals. The Thermoddem database
14
15 191 uses the Debye-Hückel theory³⁶ to calculate the activity coefficients of the ions in solution; an
16
17 192 approach that is only valid for dilute solutions. For solutions of higher salinity, such as the
18
19 193 Gassum brine, the Pitzer approach^{37, 38} to define activities based on specific ion interactions is
20
21 194 sometimes more appropriate. However, the Pitzer database only includes a limited range of
22
23 195 aqueous species and minerals, excluding many of the minerals relevant for this study.
24
25 196 The model included the thermo-kinetic processes of mineral dissolution/precipitation reaction
26
27 197 using the kinetic rate law given by^{4, 10}:

$$R = k \cdot \frac{A_0}{V} \cdot \left(\frac{m}{m_0}\right)^{0.67} \cdot (1 - \Theta) \quad (1)$$

28
29 198 where R is the dissolution/precipitation rate (mol/L/sec), k the overall rate constant (mol/m²/sec),
30
31 199 A₀ the initial surface area (m²), V the liquid volume (L), m the remaining mass of mineral, m₀ the
32
33 200 initial mass and θ the mineral saturation ratio given by $\theta = \text{IAP}/K$, where IAP is the ionic activity
34
35 201 product and K the equilibrium constant. The term $(m/m_0)^{0.67}$ corrects for changes in reactive
36
37 202 surface sites during the dissolution/precipitation process⁴.
38
39 203

40
41 204 The overall rate equation is a sum of multiple mechanisms of which those in pure water (neutral),
42
43 205 and those catalysed by H⁺ (acid) and OH⁻ (base) are included in the rate expression. The
44
45
46
47
48
49
50
51
52
53
54
55
56
57
58
59
60

1
2
3
4 206 dependency of the rate with temperature is calculated by the Arrhenius equation and the overall
5
6 207 rate constant is given by¹⁰:

7
8
9 208
$$k = k_{25}^N \exp \left[\frac{-Ea^N}{R} \left(\frac{1}{T} - \frac{1}{298.15} \right) \right] + k_{25}^A \exp \left[\frac{-Ea^A}{R} \left(\frac{1}{T} - \frac{1}{298.15} \right) \right] a_H^{n_A} + k_{25}^B \exp \left[\frac{-Ea^B}{R} \left(\frac{1}{T} - \frac{1}{298.15} \right) \right] a_H^{n_B} \quad (2)$$

10
11
12
13 209 where E_a is the activation energy (J/mol), k_{25} the rate constant at 25°C, R the gas constant
14
15 210 (J/mol/K), T the temperature (K), and a_H the activity of H^+ . The indices N , A and B refer to
16
17 211 neutral, acid and base mechanisms, respectively. For most minerals, precipitation rate data are
18
19 212 not available. Therefore, it is assumed that the same kinetic expression can be used for both
20
21 213 dissolution and precipitation processes³⁹. The initial amount of the minerals was calculated from
22
23 214 the mineral content found by the QEMSCAN[®] analysis and rate constants and the initial specific
24
25 215 surface area of the minerals were found in the literature^{39,40}. The specific reactive surface area is
26
27 216 difficult to measure or calculate since only part of the mineral surface is involved in the
28
29 217 reaction^{19,39}. For example, the hydrolysis of silicates has been shown only to occur at specific
30
31 218 sites on the surface of reactant minerals^{19,41-43}. Therefore, the specific surface area was used to
32
33 219 fit the model to the observed data. The geochemical model was fitted to the experimental data
34
35 220 from the 0.1 PV/hr experiments and subsequently tested against the results of the 0.05 PV/hr
36
37 221 experiment.

3. RESULTS AND DISCUSSION

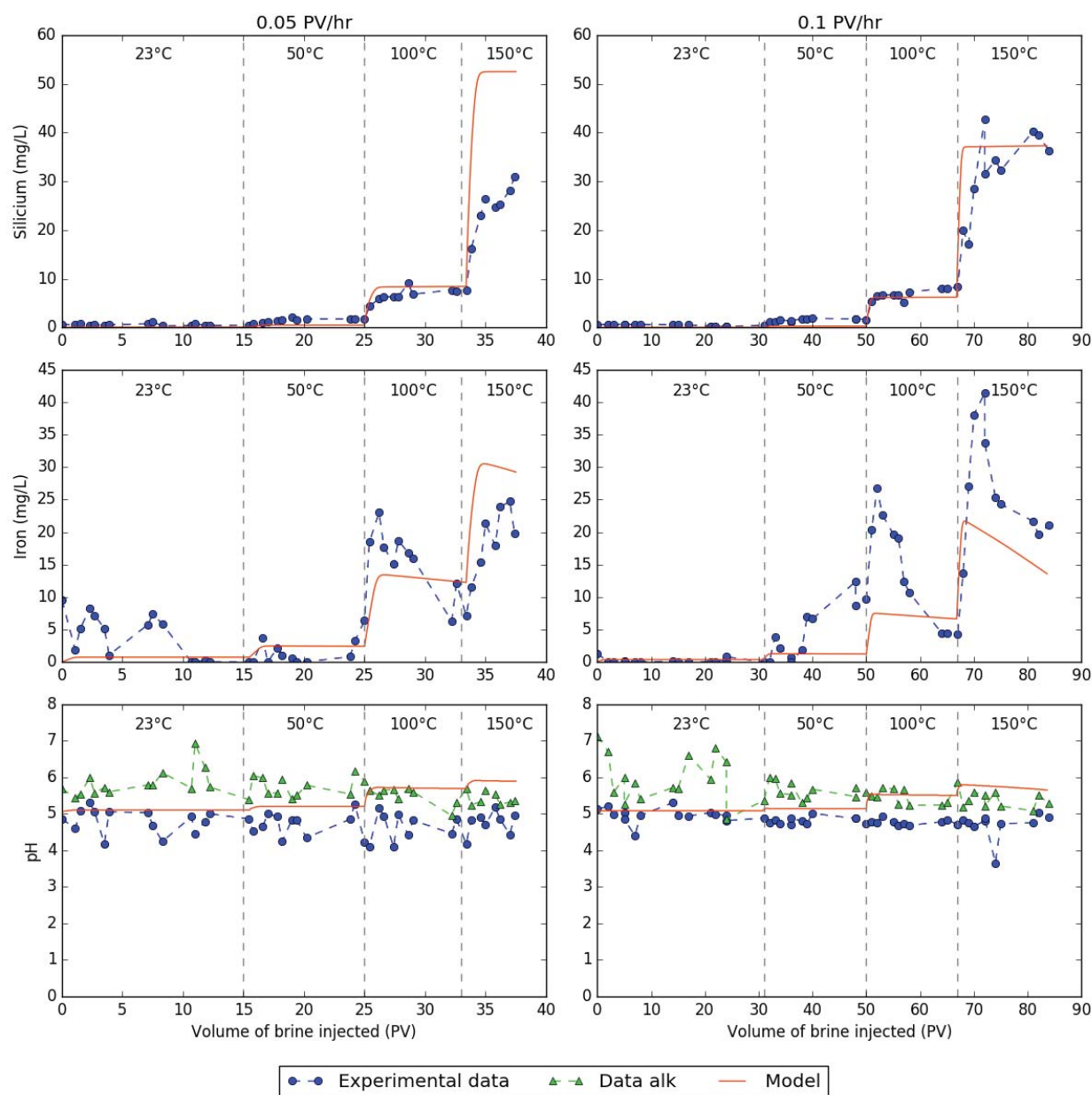
38
39
40
41
42
43
44 222 **3.1. Water chemistry.** The effects of an increasing temperature on the aqueous concentration of
45
46 223 selected parameters in the effluent are shown in Figure 3. Upon temperature increase, a clear and
47
48 224 immediate increase in the aqueous silicium concentration is observed indicating dissolution of
49
50 225 silicium bearing minerals. At each temperature, a constant level of silicium in the effluent is
51
52 226 observed, the only exception being at 150°C where the silicium concentration does not seem to
53
54
55
56
57
58
59
60

1
2
3 228 reach steady state, especially at a flow rate of 0.05 PV/hr. The plateau reached at each temperature
4
5
6 229 is identical for the two experiments, irrespective of the flow velocity, except at 150°C where a
7
8 230 lower silicium concentration is measured for the slower flow rate.
9

10
11 231 The iron concentration generally peaks immediately after an increase in the temperature followed
12
13 232 by a decreasing iron concentration. As observed for the silicium concentration, the measured iron
14
15 233 concentration is lower at 150°C for the lower flow rate as compared to the higher flow rate. Test
16
17 234 with the ferrozine method showed that the iron is present as Fe(II) indicating no or only limited
18
19 235 intrusion of oxygen to the samples.
20
21

22
23
24 236 No observable changes were identified for the concentration of chloride, sulphate, potassium,
25
26 237 calcium, magnesium and sodium, probably due to the very high content of these elements in the
27
28 238 synthetic brine and the relative small changes that any reaction would cause. Aluminium remains
29
30 239 below detection limit (0.03 mg/L) throughout the experiments (data not shown). The measured pH
31
32 240 is relatively constant between 5 and 6 at all temperatures. An accurate pH measurement was
33
34 241 difficult to obtain, since the pH drifted considerably during measurement. As a consequence both
35
36 242 the pH measured immediately after sampling and the pH at the beginning of the alkalinity
37
38 243 measurement are shown in Figure 3.
39
40
41
42

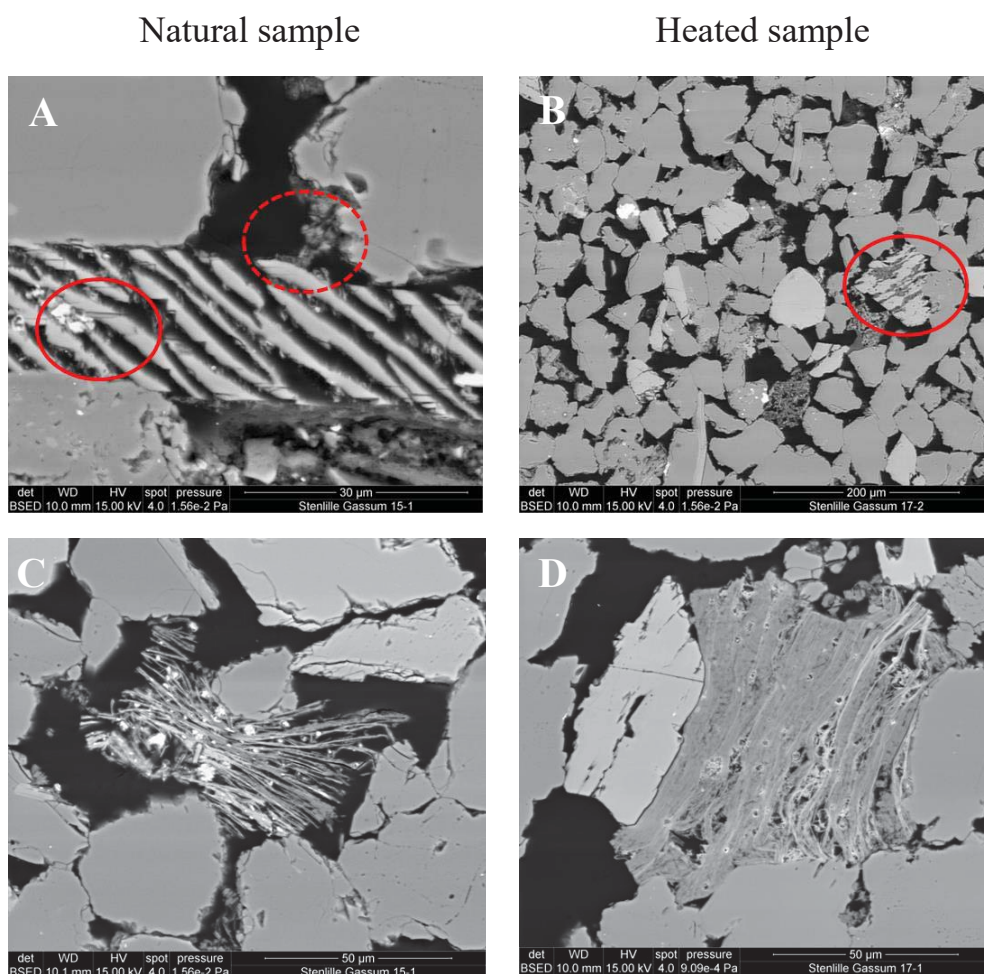
43
44 244
45
46
47
48
49
50
51
52
53
54
55
56
57
58
59
60



245
 246 **Figure 3.** Measured and modelled silicon and iron concentration and pH in the effluent of a
 247 Gassum Formation column flushed with synthetic Gassum brine (Table 1) at 23°C, 50°C (reservoir
 248 temperature), 100°C and 150°C and with a flow velocity of 0.05 PV/hr (0.014 cm/hr) and 0.1
 249 PV/hr (0.029 cm/hr). Measured data for the pH includes both the pH measurement (Experimental
 250 data) and the pH measured as the starting point in the alkalinity measurement (Data alk). The

1
2
3 251 model includes kinetically controlled dissolution/precipitation of albite, kaolinite, quartz and
4
5 252 siderite (Table 2).
6
7
8

9 253
10
11
12
13



14
15
16
17
18
19
20
21
22
23
24
25
26
27
28
29
30
31
32
33
34
35
36
37
38
39
40
41
42
43
44
45 254 **Figure 4.** Petrographic analyses of the mineralogical changes due to heating of the Gassum
46
47 255 Sandstone Formation. A: Na-rich feldspar may have been dissolved from space among K-
48
49 256 feldspar lamella in natural sample (Circle) and kaolinite precipitated (Stippled circle) B:
50
51 257 Kaolinite replacing albite in kali-feldspar in heated sample. C: Small crystal of siderite
52
53 258 associated with mica in natural sample. D: Fe-poor mica displaying holes after dissolved
54
55 259 siderite in heated sample.
56
57
58
59
60

1
2
3
4 260 **3.2. Mineralogical changes.** For the dominating quartz mineral, no changes were observed as a
5
6 261 result of flooding. As previously observed in natural samples³⁰, the Na-rich part of exsolved
7
8 262 alkalifeldspar is partly degraded and to some extent replaced by kaolinite. This process may well
9
10 263 have been promoted by the flooding experiment (Figure 4A and 4C). The flooding has caused
11
12 264 siderite to go into dissolution as evidenced by the presence of moulds after siderite crystals among
13
14 265 mica flakes (Figure 4B and 4D).

15
16
17
18 266 **3.3. Reactive transport modelling.** Based on the observed mineralogical changes as well as the
19
20 267 observed changes in the aqueous concentrations during the experiments, the geochemical model
21
22 268 was fitted to the experimental data to help identify which minerals may possibly dissolve and/or
23
24 269 precipitate when heated Gassum brine is injected into the Gassum Formation. The model optimised
25
26 270 to the experimental data includes the minerals albite (as a proxy for Na-rich alkalifeldspar),
27
28 271 kaolinite, quartz and siderite with kinetic parameters that are generally in accordance with the
29
30 272 literature (Table 2).

31
32
33
34
35 273 Even though quartz dissolution was not identified by the petrographic analysis, the reaction was
36
37 274 included in the model to reach the high silicium concentrations measured, especially at 150°C. No
38
39 275 trace of amorphous silica phases have been identified in the Gassum Formation^{27,29}. Calcite was
40
41 276 not detected by petrography or in previous studies in the Gassum Formation in the Stenlille area^{27,}
42
43 277 ²⁹ and therefore calcite is not included in the model. Simple speciation calculations show
44
45 278 subsaturation with respect to calcite in the effluent brine. Since calcite dissolution would be fast
46
47 279 compared to the residence time in the specimens, this confirms that dissolution of calcite is not
48
49 280 likely to occur in the experiment.

50
51
52
53
54
55 281
56
57
58
59
60

282 **Table 2. Specific surface area (SSA), initial mass of mineral (m_0) and kinetic parameters used**
 283 **for the reactive transport model³⁹.**

	SSA	m_0	Acid mechanisms			Neutral mechanism		Alkali mechanism		
			log(k25)	E_a	n	log(k25)	E_a	log(k25)	E_a	n
	(m ² /g)	(g)	(mol/m ² /s)	(kJ/mol)	(-)	(mol/m ² /s)	(kJ/mol)	(mol/m ² /s)	(kJ/mol)	(-)
Quartz	0.038	67.98	-	-	-	-13.99	87.7	-	-	-
Albite	0.115	0.52	-10.16	65.0	0.457	-12.56	69.8	-15.6	71.0	-0.572
Kaolinite	0.185	0.31 [†]	-11.31	65.9	0.777	-13.18	22.2	-17.05	17.9	0.472
Siderite*	$3.8 \cdot 10^{-5}$	$0.1 \cdot 10^{-2+}$	-3.19	36.1	0.500	-7.53	52.2	-5.11	34.8	0.500

*Data for siderite are assumed equivalent to dolomite⁴⁴

[†] Adjusted in the optimized model

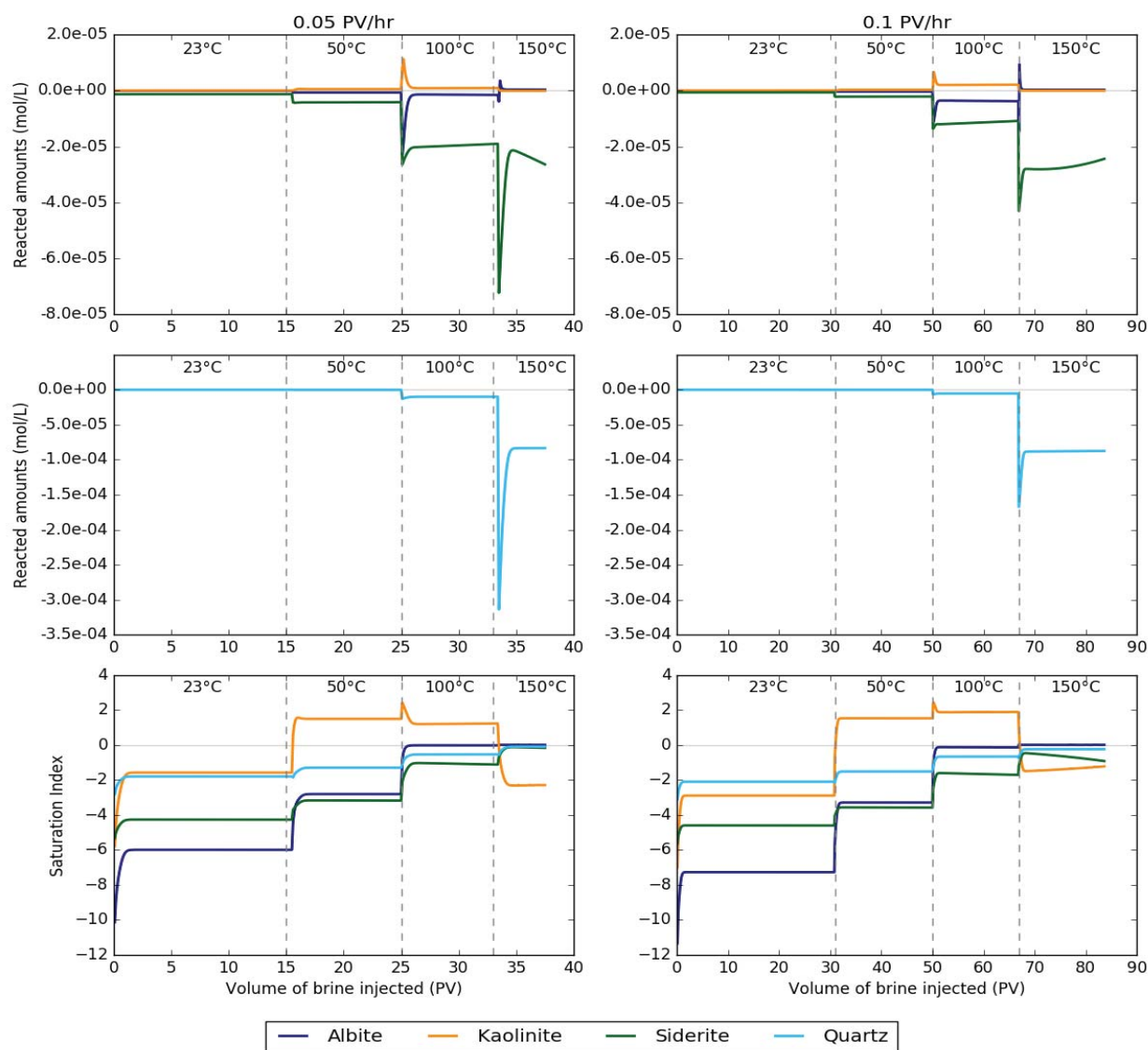
284

285 A strong coupling between Na-rich alkalifeldspar dissolution and kaolinite precipitation is
 286 observed as changes in the kaolinite precipitation rate affects the modelled aluminium and silicium
 287 concentrations. The rate of kaolinite precipitation is therefore constrained by both the silicium and
 288 aluminium concentrations. The best fit of the model to the measured data was obtained when
 289 applying a specific surface area for kaolinite of 0.185 m²/g, which is very low for typical kaolinite
 290 but within the range of previously reported values³⁹. For siderite, the best fit of the model to the
 291 measured iron concentrations was obtained by applying a specific surface area of $3.83 \cdot 10^{-5}$ m²/g.

1
2
3
4 292 Figure 3 shows the results of the geochemical model together with the experimental data for the
5
6 293 flooding experiments. The measured silicium and iron concentration as well as the pH are
7
8 294 predicted reasonably well for both experiments with the model optimised for the 0.1 PV/hr
9
10 295 experiment. Furthermore, in accordance with the measured aluminium concentrations, the model
11
12 296 predicts the aqueous aluminium concentration to be 0.01 to 0.06 mg/l and thus near the detection
13
14 297 limit (0.03 mg/L).

15
16
17
18 298 **3.4. Silicium.** For both experiments, the model reproduces the immediate increase in the silicium
19
20 299 concentration upon each temperature increase as well as the concentration level reached at each
21
22 300 temperature. The exception is the significantly lower measured silicium concentration at 150°C in
23
24 301 the 0.05 PV/hr experiment (ca. 30 mg/L) as compared to the concentration predicted by the model
25
26 302 (52 mg/L). When sampling, the effluent from the 0.1 PV/hr experiment was always sampled first,
27
28 303 leaving the sampling loop for the 0.05 PV/hr experiment at 23°C for approximately 30 min. As the
29
30 304 solubility of SiO₂ minerals decreases with decreasing temperature^{8, 45}, it is possible that a SiO₂
31
32 305 mineral, probably amorphous silica, has precipitated in the vial during this period of time, resulting
33
34 306 in a lower measured aqueous silicium concentration. Assuming the silicium concentration
35
36 307 predicted by the model in the effluent from the experiment (52 mg/L), a simple speciation
37
38 308 simulation with PHREEQC³² shows that the effluent from the 0.05 PV/hr experiment at 150°C
39
40 309 becomes slightly supersaturated with respect to amorphous silica (SI = 0.09) upon cooling to 23°C,
41
42 310 For comparison, the effluent from the 0.1 PV/hr experiment is sub-saturated with respect to
43
44 311 amorphous silica at both 150°C and upon cooling to 23°C (SI = -0.06). Precipitation of amorphous
45
46 312 silica from geothermal water has been shown to be fast (within one hour) upon cooling from 250°C
47
48 313 to 25°C⁴⁶.

1
2
3
4 314 Confirming the petrographic analysis, the model results show that at reservoir conditions (50°C)
5
6 315 dissolution of Na-rich alkali feldspar and precipitation of kaolinite occurs (Figure 5). Weathering
7
8 316 of Na-feldspar to kaolinite can be illustrated by the following reaction:



317
318 **Figure 5.** Reacted amounts and the Saturation Index for minerals included in a PHREEQC
319 transport model of synthetic Gassum brine (Table 1) through a column in which kinetically
320 controlled (Table 2) dissolution or precipitation of albite, kaolinite, siderite and quartz is allowed
321 at 0.05 PV/hr (0.014 cm/hr) and 0.1 PV/hr (0.029 cm/hr). A positive “Reacted amounts” indicates

1
2
3 322 that the mineral precipitates, while a negative value indicates dissolution of the mineral. The
4
5 323 saturation state of the effluent is indicated by the Saturation Index; the possibility of dissolution
6
7 324 and precipitation revealed by a negative and positive value of the saturation index, respectively.
8
9



14
15
16 326 Upon a temperature increase to 100°C, the conversion of feldspar to kaolinite is expected to
17
18 327 increase (Figure 5) due to a higher rate of dissolution of feldspar and precipitation of kaolinite
19
20 328 with increasing temperature^{9, 10, 47}. With increasing temperature, the solution approaches
21
22 329 saturation with respect to albite (Figure 5). Equilibrium is, however, not reached even at 100°C
23
24 330 where the simulated saturation indices for albite are -0.66 and -0.02 for the 0.1 PV/hr and 0.05
25
26 331 PV/hr experiment, respectively. The generally negative saturation indices simulated for
27
28 332 temperatures $\leq 100^\circ\text{C}$ indicate that the aqueous silicium concentration is not controlled by
29
30 333 equilibrium with either of the silicium containing mineral phases. The close to constant aqueous
31
32 334 silicium concentration measured irrespective of the flow velocity (Figure 3) suggests that the
33
34 335 silicium concentration is controlled by a quasi-stationary state between feldspar dissolution and
35
36 336 kaolinite precipitation. The flow rate affects the magnitude of the dissolution/precipitation
37
38 337 processes in this quasi-stationary state. Thus, at 100°C more feldspar is dissolved and kaolinite
39
40 338 precipitated at the higher flow as compared to the lower flow rate due to a lower saturation index
41
42 339 in the first case. These contra-intuitive results are in line with previous observations by Zhu et
43
44 340 al., (2010)⁴⁸ who found that a quasi-steady state determined by the relative rate of albite
45
46 341 dissolution and precipitation of secondary minerals was reached. In line with our results a strong
47
48 342 coupling between dissolution, precipitation and flow rates was observed. Thus depending on the
49
50 343 flow rate, the quasi steady-state was reached at different levels of saturation index⁴⁸.
51
52
53
54
55
56
57
58
59
60

1
2
3 344 With increasing temperature, dissolution of quartz becomes increasingly important, and at 100°C
4
5 345 the dissolution of quartz is in the same order of magnitude as the dissolution of Na-rich feldspar.
6
7 346 However, at 150°C the dissolution of quartz increases sharply resulting in a significant increase in
8
9 347 the aqueous silicium concentration (Figure 3). Thus, at 150°C quartz dissolution becomes the
10
11 348 predominant process, completely suppressing the dissolution of feldspar and thereby the
12
13 349 precipitation of kaolinite (Figure 5). At 150°C, the silicium concentration is solely controlled by
14
15 350 the dissolution kinetics of quartz and therefore a higher silicium concentration is predicted by the
16
17 351 model at 150°C at the velocity of 0.05 PV/hr as compared to 0.1 PV/hr.
18
19
20
21
22

23 352 **3.5. Iron.** The petrographic analysis clearly shows that dissolution of siderite occurs during the
24
25 353 flooding experiments (Figure 4). Figure 3 shows that the model reproduces the immediate increase
26
27 354 in the iron concentration upon a temperature increase followed by a decrease in the iron
28
29 355 concentration. According to the model, the decreasing iron concentration is a consequence of a
30
31 356 decrease in the siderite content as the dissolution progresses. Particularly for the 0.1 PV/hr
32
33 357 experiment, the model, however, underestimates the iron concentration. Thus, dissolution of
34
35 358 siderite may not account for all of the iron released to solution during the core flooding
36
37 359 experiments. Tests including biotite in the model do not increase the iron concentration
38
39 360 significantly. Release of iron due to corrosion of the equipment is unlikely since high corrosion-
40
41 361 resistant Hastelloy®(C-276) was used in the experimental setup. Moreover a concomitant release
42
43 362 by other elements present in the Hastelloy® in significant amounts (Ni, Cr, Mo, W, Co) was not
44
45 363 observed.
46
47
48
49
50

51 364 **4. CONCLUSION**

52
53 365 Core flooding experiments, petrographic analysis and geochemical modelling of the chemical
54
55 366 effects of heat storage of up to 150°C in the Gassum Sandstone Formation in the Stenlille area
56
57
58
59
60

1
2
3 367 show that the heating of the reservoir is expected to enhance the naturally occurring weathering of
4
5 368 Na-rich feldspar to kaolinite and induce dissolution of quartz and siderite. Assuming a constant
6
7 369 dissolution rate in the entire storage period, extrapolation of the model results indicates that less
8
9 370 than 0.05% and 0.6% of the quartz in the reservoir will dissolve during storage at 100°C or 150°C,
10
11 371 respectively, for six months and thus quartz dissolution is not expected to significantly deteriorate
12
13 372 the reservoir properties. Likewise, up to 3.2% of the Na-rich feldspar present in the reservoir will
14
15 373 dissolve during a six month storage at 100°C. Due to the small content of feldspar present in the
16
17 374 reservoir this is not expected to reduce the mechanical strength of the reservoir. The formation of
18
19 375 kaolinite will, however, increase the formation damaging potential of the reservoir as the presence
20
21 376 of even small amounts of kaolinite is known to potentially decrease the reservoir permeability
22
23 377 under certain conditions. Thus, the decline in permeability commonly observed due to heating is
24
25 378 often explained with mobilisation of colloidal particles e.g. kaolinite⁴⁹⁻⁵¹. No measureable changes
26
27 379 are, however, observed in the porosity and permeability of the tested specimens before and after
28
29 380 the experiments, indicating no formation damage of the specimens due to the flooding of heated
30
31 381 formation water (Table 3). In line with this, permeability tests with specimens from Gassum
32
33 382 Formation in the Stenlille area using synthetic brine at temperatures up to 150°C showed a small
34
35 383 permeability increase due to heating¹¹.

36
37 384 Major changes observed in the brine composition include increased silicium and iron content
38
39 385 caused by the heating induced dissolution processes. To ensure sustainable energy production from
40
41 386 the heat storage, appropriate removal of these elements e.g. by filtration in the surface facility is
42
43 387 consequently critical to prevent clogging of the injection well due to re-precipitation of silicium
44
45 388 and iron upon cooling of the brine. As the aqueous concentration of both silicium and iron
46
47 389 increases sharply above 100°C, keeping the storage temperature below 100°C, as observed at other
48
49
50
51
52
53
54
55
56
57
58
59
60

390 heat storage facilities⁵², may help reduce the chemical effects of the heat storage on the reservoir
 391 and thereby any injection problems.

392 **Table 3.** Measured porosity and gas permeability of the tested samples before and after the
 393 flooding experiments.

Sample	Flow rate (PV/hr)	Pre experiment		Post experiment	
		Porosity (%)	Permeability mD	Porosity (%)	Permeability mD
S _{0.05}	0.05	29.11 ± 0.1	195 ± 10	29.04 ± 0.1	181 ± 9
S _{0.1}	0.1	28.85 ± 0.1	181 ± 9	28.77 ± 0.1	n.a *

394 *As a small part of the S_{0.1} sample broke off during the dismantling of the sample from the core
 395 holder it was not possible to measure the permeability after the experiment.

396
 397 In conclusion, the results of this study show that the chemically induced effects of heat storage in
 398 the Gassum Formation in the Stenlille area may be of minor importance and that heat storage in
 399 the Gassum Formation in the Stenlille area may be possible provided operational precautions are
 400 taken.

401
 402 AUTHOR INFORMATION

403 **Corresponding Author**

404 *e-mail: hdh@geus.dk.

1
2
3 405 ACKNOWLEDGMENT
4

5
6 406 This research was funded by the Danish Council for Strategic Research (now Innovation Fund
7
8 407 Denmark) as part of the Heat Storage in Hot Aquifers (HeHo) project (Grant 10-093934). We
9
10 408 thank Rikke Weibel at GEUS for help with the description of the Gassum Formation and three
11
12
13 409 anonymous reviewers for their comments.
14
15

16 410

17
18 411
19
20
21
22
23
24
25
26
27
28
29
30
31
32
33
34
35
36
37
38
39
40
41
42
43
44
45
46
47
48
49
50
51
52
53
54
55
56
57
58
59
60

412 REFERENCES

- 413 (1) Lund, J. W.; Freeston, D. H.; Boyd, T. L., Direct utilization of geothermal energy 2010
414 worldwide review. *Geothermics* **2011**, *40*, (3), 159-180. DOI:
415 10.1016/j.geothermics.2011.07.004.
- 416 (2) Kabus, F.; Hofmann, F.; Möllmann, G. In *Aquifer storage of waste heat arising from a gas
417 and steam cogeneration plant - concept and first operating experience*, World Geothermal
418 Congress 2005, Antalya, Turkey, 24-29 April 2005.
- 419 (3) Réveillère, A.; Hamm, V.; Lesueur, H.; Cordier, E.; Goblet, P., Geothermal contribution to
420 the energy mix of a heating network when using Aquifer Thermal Energy Storage: Modeling and
421 application to the Paris basin. *Geothermics* **2013**, *47*, 69-79. DOI:
422 10.1016/j.geothermics.2013.02.005.
- 423 (4) Appelo, C. A. J.; Postma, D., *Geochemistry, groundwater and pollution*. 2nd ed.; A. A.
424 Balkema Publisher: 2005.
- 425 (5) Brons, H. J.; Griffioen, J.; Appelo, C. A. J.; Zehnder, A. J. B., (Bio)geochemical reactions
426 in aquifer material from a thermal-energy storage site. *Water Res.* **1991**, *25*, (6), 729-736. DOI:
427 10.1016/0043-1354(91)90048-u.
- 428 (6) Griffioen, J.; Appelo, C. A. J., Nature and extent of carbonate precipitation during aquifer
429 thermal-energy storage. *Appl. Geochem.* **1993**, *8*, (2), 161-176. DOI: 10.1016/0883-
430 2927(93)90032-c.
- 431 (7) Hoyer, M.; Hallgren, J.; Eisenreich, S.; Sterling, R., Field-test results of aquifer thermal
432 energy storage at St. Paul, Minnesota. *J. Energy Eng.* **1994**, *120*, (2), 67-85. DOI:
433 10.1061/(ASCE)0733-9402(1994)120:2(67).
- 434 (8) Dove, P. M.; Crerar, D. A., Kinetics of quartz dissolution in electrolyte solutions using a
435 hydrothermal mixed flow reactor. *Geochim. Cosmochim. Acta* **1990**, *54*, (4), 955-969. DOI:
436 10.1016/0016-7037(90)90431-J.
- 437 (9) Gruber, C.; Kutuzov, I.; Ganor, J., The combined effect of temperature and pH on albite
438 dissolution rate under far-from-equilibrium conditions. *Geochim. Cosmochim. Acta* **2016**, *186*,
439 154-167. DOI: 10.1016/j.gca.2016.04.046.
- 440 (10) Palandri, J. L.; Kharaha, Y. K. *A compilation of rate parameters of water-mineral
441 interaction kinetics for application to geochemical modeling*; U.S. Geological Survey Water-
442 Resources Investigations Report 04-1068, 2004.
- 443 (11) Holmslykke, H. D.; Kjøller, C.; Fabricius, I. L., The effect of heating and flow velocity on
444 the permeability in the Gassum and Bunter Sandstone Formations. **In prep.**
- 445 (12) Tenthorey, E.; Scholz, C. H.; Aharonov, E.; Leger, A., Precipitation sealing and
446 diagenesis - 1. Experimental results. *J. Geophys. Res.: Solid Earth* **1998**, *103*, (B10), 23951-
447 23967. DOI: 10.1029/98jb02229.
- 448 (13) Moore, D. E.; Morrow, C. A.; Byerlee, J. D., Chemical reactions accompanying fluid flow
449 through granite held in a temperature gradient. *Geochim. Cosmochim. Acta* **1983**, *47*, (3), 445-
450 453. DOI: 10.1016/0016-7037(83)90267-3.
- 451 (14) Bonte, M.; Stuyfzand, P. J.; van Breukelen, B. M., Reactive transport modeling of thermal
452 column experiments to investigate the impacts of aquifer thermal energy storage on groundwater
453 quality. *Environ. Sci. Technol.* **2014**, *48*, (20), 12099-12107. DOI: 10.1021/es502477m.
- 454 (15) Possemiers, M.; Huysmans, M.; Batelaan, O., Influence of aquifer thermal energy storage
455 on groundwater quality: A review illustrated by seven case studies from Belgium. *J. Hydrol.
456 Reg. Stud.* **2014**, *2*, 20-34. DOI: 10.1016/j.ejrh.2014.08.001.

- 1
2
3
4 457 (16) Perlinger, J. A.; Almendinger, J. E.; Urban, N. R.; Eisenreich, S. J., Groundwater
5 458 geochemistry of aquifer thermal energy storage - Long term test cycle. *Water Resour. Res.* **1987**,
6 459 23, (12), 2215-2226. DOI: 10.1029/WR023i012p02215.
- 7 460 (17) Vetter, A.; Mangelsdorf, K.; Schettler, G.; Seibt, A.; Wolfgramm, M.; Rauppach, K.;
8 461 Vieth-Hillebrand, A., Fluid chemistry and impact of different operating modes on microbial
9 462 community at Neubrandenburg heat storage (Northeast German Basin). *Org. Geochem.* **2012**, *53*,
10 463 8-15. DOI: 10.1016/j.orggeochem.2012.08.008.
- 11 464 (18) Holmslykke, H. D.; Kjøller, C.; Fabricius, I. L., Core flooding experiments and reactive
12 465 transport modelling of heat storage in the Bunter Sandstone Formation. **In prep.**
- 13 466 (19) Azaroual, M.; Fouillac, C., Experimental study and modelling of granite-distilled water
14 467 interactions at 180 degrees C and 14 bars. *Appl. Geochem.* **1997**, *12*, (1), 55-73. DOI:
15 468 10.1016/s0883-2927(96)00054-6.
- 16 469 (20) Schepers, A.; Milsch, H., Dissolution-precipitation reactions in hydrothermal experiments
17 470 with quartz-feldspar aggregates. *Contrib. Mineral. Petrol.* **2013**, *165*, (1), 83-101. DOI:
18 471 10.1007/s00410-012-0793-x.
- 19 472 (21) Gong, Q.; Deng, J.; Han, M.; Yang, L.; Wang, W., Dissolution of sandstone powders in
20 473 deionised water over the range 50–350 °C. *Appl. Geochem.* **2012**, *27*, (12), 2463-2475. DOI:
21 474 10.1016/j.apgeochem.2012.08.011.
- 22 475 (22) Fu, Q.; Lu, P.; Konishi, H.; Dilmore, R.; Xu, H.; Seyfried Jr, W. E.; Zhu, C., Coupled
23 476 alkali-feldspar dissolution and secondary mineral precipitation in batch systems: 1. New
24 477 experiments at 200 °C and 300 bars. *Chem. Geol.* **2009**, *258*, (3–4), 125-135. DOI:
25 478 10.1016/j.chemgeo.2008.09.014.
- 26 479 (23) Nielsen, L. H., Late Triassic-Jurassic development of the Danish Basin and the
27 480 Fennoscandian Border Zone, southern Scandinavia. In *The Jurassic of Denmark and Greenland*,
28 481 Ineson, J. R.; Surlyk, F., Eds. Geological Survey of Denmark and Greenland Bulletin 1, 2003; pp
29 482 459-526.
- 30 483 (24) Nielsen, L. H.; Japsen, P. *Deep wells in Denmark 1935-1990. Lithostratigraphic*
31 484 *subdivision*; Geological Survey of Denmark A 31, 1991; p 179 pp.
- 32 485 (25) Laier, T.; Øbro, H., Environmental and safety monitoring of the natural gas underground
33 486 storage at Stenlille, Denmark. In *Underground gas storage: Worldwide experiences and future*
34 487 *development in the UK and Europe.*, Evans, D. J.; Chadwick, R. A., Eds. The Geological
35 488 Society, London, Special Publication, 2009; Vol. 313, pp 81-92.
- 36 489 (26) Liboriussen, J.; Ashton, P.; Thygesen, T., The tectonic evolution of the Fennoscandian
37 490 Border Zone in Denmark. In *Compressional intraplate deformations in the Alpine Foreland*,
38 491 Ziegler, P. A., Ed. Tectonophysics, 1987; Vol. 137, pp 21-29.
- 39 492 (27) Friis, H. *Diagenesis of the Gassum Formation Rhaetian-Lower Jurassic, Danish*
40 493 *Subbasin*; Geological Survey of Denmark A 18: 1987; p 41pp.
- 41 494 (28) McBride, E. F., A classification of common sandstones. *J. Sediment. Petrol.* **1963**, *33*,
42 495 664-669.
- 43 496 (29) Weibel, R.; Olivarius, M.; Kristensen, L.; Friis, H.; Hjuler, M. L.; Kjøller, C.; Mathiesen,
44 497 A.; Nielsen, L. H., Predicting permeability of low-enthalpy geothermal reservoirs: A case study
45 498 from the Upper Triassic – Lower Jurassic Gassum Formation, Norwegian–Danish Basin.
46 499 *Geothermics* **2017**, *65*, 135-157. DOI: 10.1016/j.geothermics.2016.09.003.
- 47 500 (30) Weibel, R.; Olivarius, M.; Nielsen, L. H.; Abramovitz, T.; Kjoller, C. *Petrography and*
48 501 *diagenesis of the Triassic and Jurassic sandstones, eastern part of the Norwegian-Danish Basin*;
49 502 Geological Survey of Denmark and Greenland report 114: 2010; p 88pp.
- 50
51
52
53
54
55
56
57
58
59
60

- 1
2
3
4 503 (31) Laier, T. *Chemistry of Danish saline formation waters relevant for core fluid experiments*
5 504 – *Fluid chemistry data for lab experiments related to CO₂ storage on deep aquifers*; GEUS
6 505 report 2008/48: 2008.
- 7 506 (32) Parkhurst, D. L.; Appelo, C. A. J., *Description of input and examples for PHREEQC*
8 507 *version 3 - A computer program for speciation, batch-reaction, one-dimensional transport, and*
9 508 *inverse geochemical calculations*. U.S. Geological Survey Techniques and Methods, 2013; Vol.
10 509 book 5, chap. A43, 497 p. Available only at <http://pubs.usgs.gov/tm/06/a43/>.
- 11 510 (33) Blanc, P.; Lassin, A.; Piantone, P. Thermodem: A database devoted to waste minerals.
12 511 <http://thermoddem.brgm.fr/>
- 13 512 (34) API, *Recommended practice for core analysis - Recommended practice 40, second*
14 513 *edition*. American Petroleum Institute: Washington DC, 1998; p 236.
- 15 514 (35) Stumm, W.; Morgan, J. J., *Aquatic Chemistry*. John Wiley, N. Y., 1981.
- 16 515 (36) Atkins, P. W.; de Paula, J., *Atkins' physical chemistry*. 7th ed.; oxford Univ. Press, 2002.
- 17 516 (37) Pitzer, K. S., Characteristics of very concentrated aqueous solutions. *Physics and*
18 517 *Chemistry of the Earth* **1981**, *13*, 249-272. DOI: 10.1016/0079-1946(81)90013-6.
- 19 518 (38) Plummer, L. N.; Parkhurst, D. L.; Fleming, G. W.; Dunkle, S. A. *A computer program*
20 519 *incorporating Pitzer's equations for calculation of geochemical reactions in brines*; 88-4153;
21 520 1988.
- 22 521 (39) Cantucci, B.; Montegrossi, G.; Vaselli, O.; Tassi, F.; Quattrocchi, F.; Perkins, E. H.,
23 522 *Geochemical modeling of CO₂ storage in deep reservoirs: The Weyburn Project (Canada) case*
24 523 *study*. *Chem. Geol.* **2009**, *265*, (1–2), 181-197. DOI: 10.1016/j.chemgeo.2008.12.029.
- 25 524 (40) André, L.; Audigane, P.; Azaroual, M.; Menjoz, A., Numerical modeling of fluid–rock
26 525 chemical interactions at the supercritical CO₂–liquid interface during CO₂ injection into a
27 526 carbonate reservoir, the Dogger aquifer (Paris Basin, France). *Energy Convers. Manage.* **2007**,
28 527 *48*, (6), 1782-1797. DOI: 10.1016/j.enconman.2007.01.006.
- 29 528 (41) Chou, L.; Wollast, R., Study of the weathering of albite at room-temperature and pressure
30 529 with a fluidized-bed reactor. *Geochim. Cosmochim. Acta* **1984**, *48*, (11), 2205-2217. DOI:
31 530 10.1016/0016-7037(84)90217-5.
- 32 531 (42) Berner, R. A.; Holdren, G. R., Mechanism of feldspar weathering 2. Observations of
33 532 feldspars from soils. *Geochim. Cosmochim. Acta* **1979**, *43*, (8), 1173-1186. DOI: 10.1016/0016-
34 533 7037(79)90110-8.
- 35 534 (43) Holdren, G. R.; Speyer, P. M., Reaction rate-surface area relationships during the early
36 535 stages of weathering 1. Initial observations. *Geochim. Cosmochim. Acta* **1985**, *49*, (3), 675-681.
37 536 DOI: 10.1016/0016-7037(85)90162-0.
- 38 537 (44) Gunter, W. D.; Perkins, E. H.; Hutcheon, I., Aquifer disposal of acid gases: modelling of
39 538 water–rock reactions for trapping of acid wastes. *Appl. Geochem.* **2000**, *15*, (8), 1085-1095. DOI:
40 539 10.1016/S0883-2927(99)00111-0.
- 41 540 (45) Rimstidt, J. D.; Barnes, H. L., The kinetics of silica-water reactions. *Geochim.*
42 541 *Cosmochim. Acta* **1980**, *44*, (11), 1683-1699. DOI: 10.1016/0016-7037(80)90220-3.
- 43 542 (46) Dixit, C.; Bernard, M.-L.; Sanjuan, B.; André, L.; Gaspard, S., Experimental study on the
44 543 kinetics of silica polymerization during cooling of the Bouillante geothermal fluid (Guadeloupe,
45 544 French West Indies). *Chem. Geol.* **2016**, *442*, 97-112. DOI: 10.1016/j.chemgeo.2016.08.031.
- 46 545 (47) Manning, D. A. C., Experimental studies of clay mineral occurrence. In *Clay mineral*
47 546 *cements in sandstones (Special publication number 34 of the international association of*
48 547 *sedimentologists)*, Worden, R. H.; Morad, S., Eds. Blackwell publishing: 2003; pp 177-190.

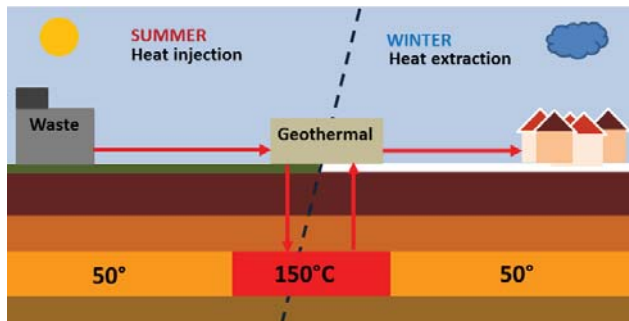
- 1
2
3
4 548 (48) Zhu, C.; Lu, P.; Zheng, Z.; Ganor, J., Coupled alkali feldspar dissolution and secondary
5 549 mineral precipitation in batch systems: 4. Numerical modeling of kinetic reaction paths.
6 550 *Geochim. Cosmochim. Acta* **2010**, *74*, (14), 3963-3983. DOI: 10.1016/j.gca.2010.04.012.
7 551 (49) Rosenbrand, E.; Haugwitz, C.; Jacobsen, P. S. M.; Kjoller, C.; Fabricius, I. L., The effect
8 552 of hot water injection on sandstone permeability. *Geothermics* **2014**, *50*, 155-166. DOI:
9 553 10.1016/j.geothermics.2013.09.006.
10 554 (50) Rosenbrand, E.; Kjoller, C.; Riis, J. F.; Kets, F.; Fabricius, I. L., Different effects of
11 555 temperature and salinity on permeability reduction by fines migration in Berea sandstone.
12 556 *Geothermics* **2015**, *53*, 225-235. DOI: 10.1016/j.geothermics.2014.06.004.
13 557 (51) Schembre, J. M.; Kovscek, A. R., Mechanism of formation damage at elevated
14 558 temperature. *J. Energy Resour. Technol. Trans. ASME* **2005**, *127*, (3), 171-180. DOI:
15 559 10.1115/1.1924398.
16 560 (52) Kabus, F.; Wolfgramm, M. In *Aquifer thermal energy storage in Neubrandenburg-*
17 561 *monitoring throughout three years of regular operation*, Proceedings of the 11th international
18 562 conference on energy storage 2009, Stockholm, Sweden, 2009; p 8pp.

21
22 56323 564
24
25
26
27
28
29
30
31
32
33
34
35
36
37
38
39
40
41
42
43
44
45
46
47
48
49
50
51
52
53
54
55
56
57
58
59
60

1
2
3
4
5
6
7
8
9
10
11
12
13
14
15
16
17
18
19
20
21
22
23
24
25
26
27
28
29
30
31
32
33
34
35
36
37
38
39
40
41
42
43
44
45
46
47
48
49
50
51
52
53
54
55
56
57
58
59
60

565 **For table of contents only**

566



567

568